AGU PUBLICATIONS

Geophysical Research Letters

RESEARCH LETTER
10.1002/2015GL066544

Key Points:
- Smoke interacting with cloud delays the transition via suppression of precipitation
- An elevated smoke layer with high moisture hastens the stratocumulus to cumulus transition
- The delayed transition results in larger areal cover and stronger forcing by the stratocumulus deck

Correspondence to:
T. Yamaguchi,
tak.yamaguchi@noaa.gov

Citation:
Yamaguchi, T., G. Feingold, J. Kazil, and A. McComiskey (2015), Stratocumulus to cumulus transition in the presence of elevated smoke layers, *Geophys. Res. Lett.*, *42*, 10,478–10,485, doi:10.1002/2015GL066544.

Received 9 OCT 2015
Accepted 17 NOV 2015
Accepted article online 24 NOV 2015
Published online 11 DEC 2015

Stratocumulus to cumulus transition in the presence of elevated smoke layers

Takanobu Yamaguchi[1,2], Graham Feingold[2], Jan Kazil[1,2], and Allison McComiskey[2]

[1]Cooperative Institute for Research in Environmental Sciences, University of Colorado Boulder, Boulder, Colorado, USA, [2]NOAA Earth System Research Laboratory, Boulder, Colorado, USA

Abstract The transition from stratocumulus to cumulus clouds in the presence of elevated light-absorbing smoke layers is investigated with idealized large-eddy simulations. A smoke layer is placed 1 km above stratocumulus top and evolves with the cloud fields over the course of a 3 day simulation. The simulations presented vary the smoke-generated heating and the moisture content of the smoke layer. A control case without smoke is simulated for comparison. On day 2 of the transition, when still above cloud, smoke generates a more broken cloud field than the control case, depending weakly on the strength of the aerosol heating but strongly on the water vapor content in the smoke layer. Following nighttime recovery and contact with the stratocumulus, smoke hinders the transition by strengthening the inversion, limiting boundary layer deepening and reducing precipitation-related breakup. This modulation delays the transition, which may extend the stratocumulus deck westward, with concomitant implications for climate forcing.

1. Introduction

The transition from stratocumulus to cumulus (SCT) clouds over the subtropical oceans is a topic of wide interest for climate studies. Given that the SCT is primarily driven by advection of the cloud system over a progressively warming sea surface temperature (SST) [e.g., *Bretherton*, 1992; *Krueger et al.*, 1995; *Wyant et al.*, 1997; *Sandu et al.*, 2010], the SCT encapsulates not only fundamental elements of the cloudy boundary layer but also cloud feedbacks in a warmer SST world.

The subject of the SCT has already been the focus of extensive study. A conceptual model of SCT linked to increasing SST and latent heat fluxes, boundary layer decoupling, conditional instability in the lower boundary layer, penetrative cumulus, and a thinning and drying stratocumulus layer has been proposed [*Bretherton*, 1992], with later studies confirming the fundamental mechanisms [*Wyant et al.*, 1997]. *Sandu et al.* [2010] analyzed a large number of reanalysis-derived trajectories to explore the meteorological conditions associated with the transition. They showed that composites of trajectories in a number of ocean basins share essential characteristics, suggesting that the underlying processes behind SCT are robust and not subject to significant contingency.

Based on this trajectory analysis, *Sandu and Stevens* [2011, henceforth SS11] developed a case study that represents the key aspects of the transition in the North East Pacific. For their composite case, the SCT typically takes place within 3 days but they also examined the conditions associated with outliers and showed that the time scale of the SCT is proportional to the lower tropospheric stability (LTS). The SCT was also dependent to a somewhat lesser degree on free tropospheric water vapor, the presence of which tends to modify the nature of the SCT, e.g., cloud amount, but not the rate of the SCT.

The SCT in the South East Atlantic region has the added dimension of occurring in the presence of smoke associated with the world's largest source of biomass burning aerosol from the African subcontinent. Interest in this region is reflected in the number of large international and multiagency field campaigns (CLouds and Aerosol Radiative Impacts and Forcing: Year 2016, CLARIFY-2016; Layered Atlantic Smoke Interactions with Clouds, LASIC; and ObseRvations of Aerosols above CLouds and their intEractionS, ORACLES) planned for the coming years to study the transport and transformation of the smoke, its interaction with clouds, and the radiative impacts on the system—all within a relatively poorly studied part of the world.

The smoke is seasonally transported out over the South East Atlantic, typically some distance above the stratocumulus cloud deck, and often accompanied by moisture associated with continental outflow [*Adebiyi et al.*, 2015]. Even in the absence of direct smoke-cloud contact, the heat absorbed by the aerosol during the day represents an intermittent remote radiative forcing on the cloud system below that varies with solar zenith angle and changes spatially as a function of smoke source strength/distribution and prevailing winds. This is in contrast to the much more homogeneous surface heat source that the system experiences with progressive westward transport over warmer SSTs. While toward the east the smoke may initially reside some distance above the cloud, a combination of a deepening boundary layer as the system moves westward over warmer SSTs and subsidence bring the smoke and clouds into contact and allow for microphysical interactions in addition to radiative interactions. The coupled nature of the system provides the potential for a rich set of responses.

The influence of the smoke on SCT has not, to our knowledge, been studied with process models. A number of earlier modeling studies have addressed the influence of smoke in or immediately above a stratocumulus layer [*Johnson et al.*, 2004; *Hill and Dobbie*, 2008] or cumulus layer [*Ackerman et al.*, 2000; *Johnson*, 2005; *Feingold et al.*, 2005]. The influence of smoke on boundary layer clouds has also been studied with observations [e.g., *Wilcox*, 2010, 2012; *Painemal et al.*, 2014]. The understanding emerging from these studies is that smoke aerosol residing just above stratocumulus clouds tends to strengthen the inversion, weaken entrainment, and generate a stronger cloud radiative effect (CRE), while smoke residing within the boundary layer tends to heat the boundary layer and reduce cloudiness and the CRE. The influence of elevated smoke layers on the SCT is uncertain.

The consistency in the transitions across ocean basins highlighted by *Sandu et al.* [2010] suggests that idealized numerical experiments addressing SCT using the SS11 case based on the North East Pacific trajectories are of relevance to the South East Atlantic. The current study therefore explores some of the expected roles of light-absorbing smoke on the transition using the SS11 case but with the addition of elevated smoke and/or moist layers. The simulations are far from exhaustive and await the measurement campaigns for more specific cases studies. Nevertheless, they highlight some of the interesting roles that smoke aerosol can play in the SCT.

2. Simulations

The System for Atmospheric Modeling [*Khairoutdinov and Randall*, 2003] is configured for the 3 day Lagrangian SCT case of SS11. The domain size is $12\times12\times4.25$ km^3 and the grid volume is $50\times50\times10$ m^3 below 2.775 km with vertical grid stretching above. Radiation is computed with the rapid radiative transfer model (RRTM) [*Mlawer et al.*, 1997] with extended profiles added above the domain top to represent the full atmospheric column. The cloud microphysics is a two-moment bin-emulating method [*Feingold et al.*, 1998] that calculates mass and number mixing ratios of both cloud and raindrops and also calculates supersaturation. SST forcing follows SS11, and subsidence follows *Bretherton and Blossey* [2014]. Surface fluxes are computed based on similarity theory.

The simulations include a coupled aerosol model that allows for spatially and temporally (diurnal cycle) varying heating rates. The aerosol model accounts for both the cloud nucleating and absorbing components of the aerosol [*Feingold et al.*, 2005]. A prognostic equation is solved for aerosol number concentration, n_a; particles are advected and diffused, removed upon droplet nucleation, regenerated after droplet evaporation, and reduced in concentration through coalescence scavenging or surface precipitation. The size distribution is assumed to be invariant (a lognormal function with median radius of 0.1 μm and geometric standard deviation of 1.5). The hygroscopic fraction of the aerosol is assumed to be ammonium sulfate, and the nonhygroscopic, absorbing part is black carbon. This same aerosol representation is used to generate a priori look up tables of humidity-dependent optical properties (single scattering albedo, ω_o, asymmetry parameter, and extinction coefficient) for unit n_a so that local heating rates can be computed by the radiation code and applied during model simulation.

Two smoke optical property look up tables are prepared: strongly absorbing particles ($\omega_o = 0.8$ at relative humidity (RH) of 0.7 at 533 nm) and weakly absorbing particles ($\omega_o = 0.94$). A 1 km deep smoke layer ($1905\ \text{m} \le z \le 2905$ m) is inserted with its base located approximately 1 km above initial cloud top (885 m) (Figure 2a, circle). For the cases simulated, this results in smoke encountering the cloud roughly halfway through the simulation ($t \approx 38$ h). The smoke n_a is calculated based on an aerosol optical depth, τ_a, of 0.5

(at 533 nm) in the smoke layer, taking into account aerosol uptake of water vapor. The background n_a is 150 mg^{-1} (150 cm^{-3} at an air density of 1 kg m^{-3}), which gives $\tau_a \approx 0.1$ below the smoke layer for both smoke types. A surface particle flux of 70 cm^{-2} s^{-1} is applied for all simulations to sustain reasonable background n_a [*Wang et al.*, 2010]. For convenience, the composition of the background aerosol and thus the optical properties are assumed to be the same as that of the smoke. While this is unrealistic, it is of no practical consequence because of the low background n_a compared to the large smoke concentrations noted below.

To mimic the observed enhanced moisture in the smoke layer, a moist layer is optionally placed between 1905 m and 2905 m (i.e., the same as the smoke layer). The vapor mixing ratio in the moist layer is specified at 7.5 g kg^{-1} compared to 3.4–3.8 g kg^{-1} immediately above and below, and the RH increases from ≈ 0.25 to ≈ 0.5. St. Helena soundings often show RH exceeding 0.5, approximately coincident with the smoke layer for $\tau_a > 0.2$, and the moisture in the smoke layer is typically ≈ 3 g kg^{-1} with a maximum of ≈ 6 g kg^{-1} [*Adebiyi et al.*, 2015]. The specified moist layer vapor amount is admittedly unrealistic, and the effect associated with the moist layer should be seen as an upper limit.

The control case (Control) includes neither a smoke layer nor a moist layer. Two simulations include a smoke layer aloft and differ only in ω_o: SMK1 is used to denote the strongly absorbing aerosol ($\omega_o = 0.8$) and SMK2 the weakly absorbing aerosol ($\omega_o = 0.94$). MST-R is the same as Control but with a stationary moist layer that is only used for radiative calculations. The last case, SMK2-QV is the same as SMK2 but with an evolving moist layer initially collocated with the smoke layer. For these smoke cases, $\tau_a = 0.5$ translates to $n_a = 5882$ mg^{-1} for SMK1, 6390 mg^{-1} for SMK2, and 4779 mg^{-1} for SMK2-QV. The mean daytime shortwave heating rate due to the smoke layer when it is separated from the cloud (before 38 h) is approximately 4 K d^{-1} for SMK1, 1.2 K d^{-1} for SMK2, and 1.1 K d^{-1} for SMK2-QV.

3. Results

3.1. Control

The diurnal evolution for Control shown in Figure 1 is similar to the corresponding simulation of SS11 (their REF case) and *Bretherton and Blossey* [2014] (their CTLD case). The diurnal evolution includes (i) daytime cloud breakup and evaporation accompanied by slow rise of the inversion height (z_i) (24 h–31 h and 49 h–56 h) and weakening turbulence and (ii) nighttime recovery of cloud fraction (f_c, calculated based on cloud optical depth $\tau_c > 2$), cloud water path (CWP, average of both cloudy and clear columns), and turbulence kinetic energy (TKE) accompanied by faster boundary layer deepening (Figures 1a–1c and 1f). During the third night, the deeper boundary layer supports higher local concentrations of liquid water. Thereafter, rain water path and TKE increase in unison indicating SCT through precipitation (Figure 1ef) [e.g., *Wang et al.*, 1993], which differs from the above mentioned studies. We note that in our simulations this precipitation-associated transition does not occur in a 6×6 km^2 horizontal domain, and it occurs earlier in a 24×24 km^2 domain. Thus, domain size clearly influences the SCT; however, this is outside of the scope of the current study.

3.2. Smoke Layer Cases: SMK1 and SMK2

Many of the cloud and boundary layer fields for these two smoke layer cases evolve much like Control prior to 38 h; on day 2, f_c is ≈ 0.1 less than Control, accompanied by minor reductions in CWP and z_i from slightly weaker net cloud top cooling rates (Figures 1a–1c and 2g, circle).

After the cloud makes contact with the smoke ($t > 38$ h) SMK1 and SMK2 exhibit a distinct slowing in the rate of growth of z_i (Figure 1c) because of the increased stability at z_i (Figures 1g and 2b, diamond) generated by the smoke layer shortwave (SW) heating over the previous day [*Johnson et al.*, 2004]. As expected, the smaller ω_o (SMK1) results in a more stable inversion and weaker growth in z_i. When smoke makes contact with cloud, there is a significant increase in the mean droplet number concentration, n_c; differences between SMK1 and SMK2 are due to differences in smoke layer SW heating, which influences how much smoke is entrained (Figure 1d). The smoke layers evolve and dilute through diffusion and positive buoyancy generated by the internal heat source (Figure 2a). SMK1 is able to develop noticeable turbulence through buoyant production of TKE (TKE_B) between 2.5 km and 3 km inside the smoke layer (Figure 2h), which significantly reduces the n_a available for entrainment. Thus, the concentration of the entrained smoke will depend not only on upstream emission strength but also on ω_o and tropospheric stability.

By day 3, smoke heating has strengthened the inversion (Figure 1g), resulting in $f_c \approx 1$, i.e., higher than Control. Overall, these smoke cases result in a shallower boundary layer, higher f_c, and a delay in the SCT. The delay

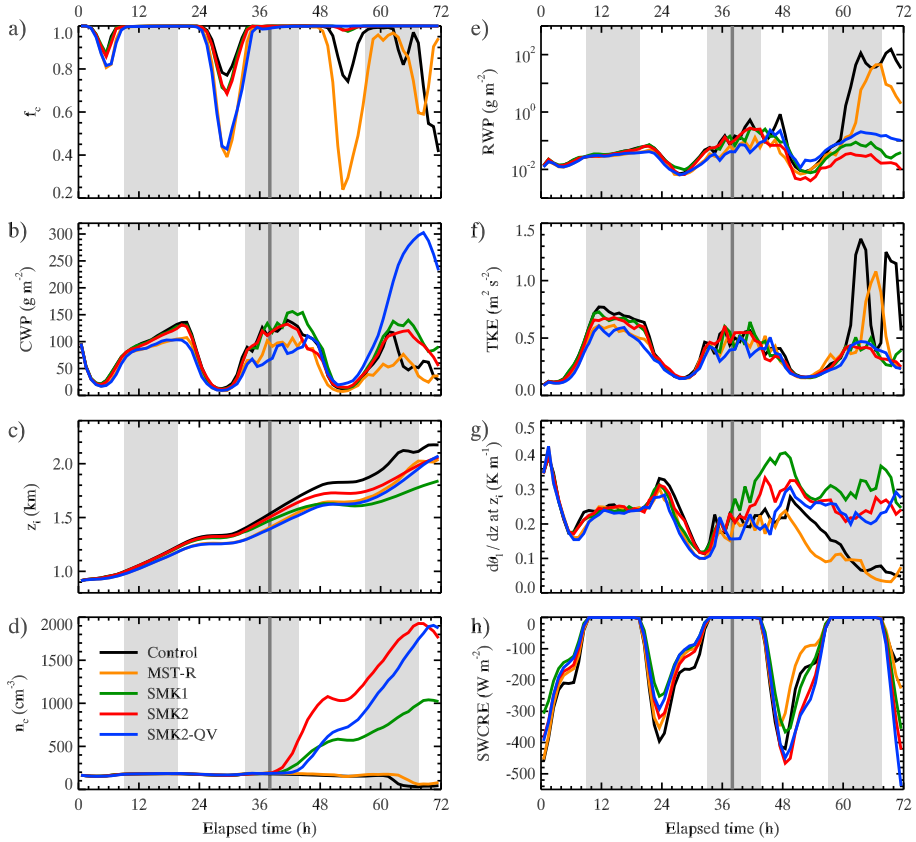

Figure 1. Time series of selected hourly averaged variables for five cases. Variables are described in the text. z_i is defined as the mean height of the largest vertical gradient of liquid water potential temperature, θ_l. n_c is computed as a cloudy-column average of cloud layer mean droplet number concentration. The cloud base (top) is identified at the lowest (highest) level with cloud water content of 0.01 g kg $^{-1}$. Stability ($d\theta_l/dz$) at z_i is calculated based on horizontal mean θ_l. Here TKE is the vertical mean TKE computed below z_i. Night is represented by light gray shading. Smoke interacts with cloud approximately after 38 h as shown by the vertical dark gray line.

results from a combination of a shallower boundary layer, which prevents deeper, wetter clouds (a dynamical response), as well as microphysical suppression of rain.

3.3. Moist Layer Case: MST-R

The stationary moist layer case (MST-R) exhibits amplified daytime cloud evaporation and lower CWP and z_i than Control (Figures 1a–1c) through modulation of the radiative heating associated with the moist layer some distance above the cloud. The moist layer weakens the cloud top longwave (LW) cooling by increasing the downward LW flux at the cloud top [*Wang et al*., 1993; SS11] (discussed further in section 3.4). During the third night, before fully recovering, f_c starts to decrease as a result of precipitation-induced SCT. An additional simulation with a dynamically evolving moist layer (not shown) that allows vapor to subside down to the cloud layer mimics the behavior of MST-R prior to 38 h, but by day 3 (~50 h) when the moisture encounters the cloud, f_c approaches 1. The SCT occurs during the third night for Control and MST-R (as well as the evolving moist layer case). This insensitivity of the *timing* of SCT to the moist layer is consistent with SS11.

3.4. Influence of Moisture and Smoke Layer Aloft: SMK2-QV and MST-R; $t < 38$ h

Compared with Control, key differences for MST-R and SMK2-QV before 38 h are (i) large daytime reductions in f_c (Figure 1a) and (ii) lower CWP and TKE (particularly at night) and lower z_i (Figures 1b, 1c, and 1f). SMK2-QV closely tracks MST-R before 38 h. It is only the modification of cloud top radiative heating rate due to the presence of the elevated smoke layer that is responsible for these differences from Control, and the moisture in the smoke layer is the dominant contributor to the modulation as explained below.

As noted above, the moisture in the elevated smoke layer weakens the cloud top longwave (LW) cooling. Smoke is radiatively inactive in the LW. The cloud top SW heating is, to first order, only weakly sensitive to

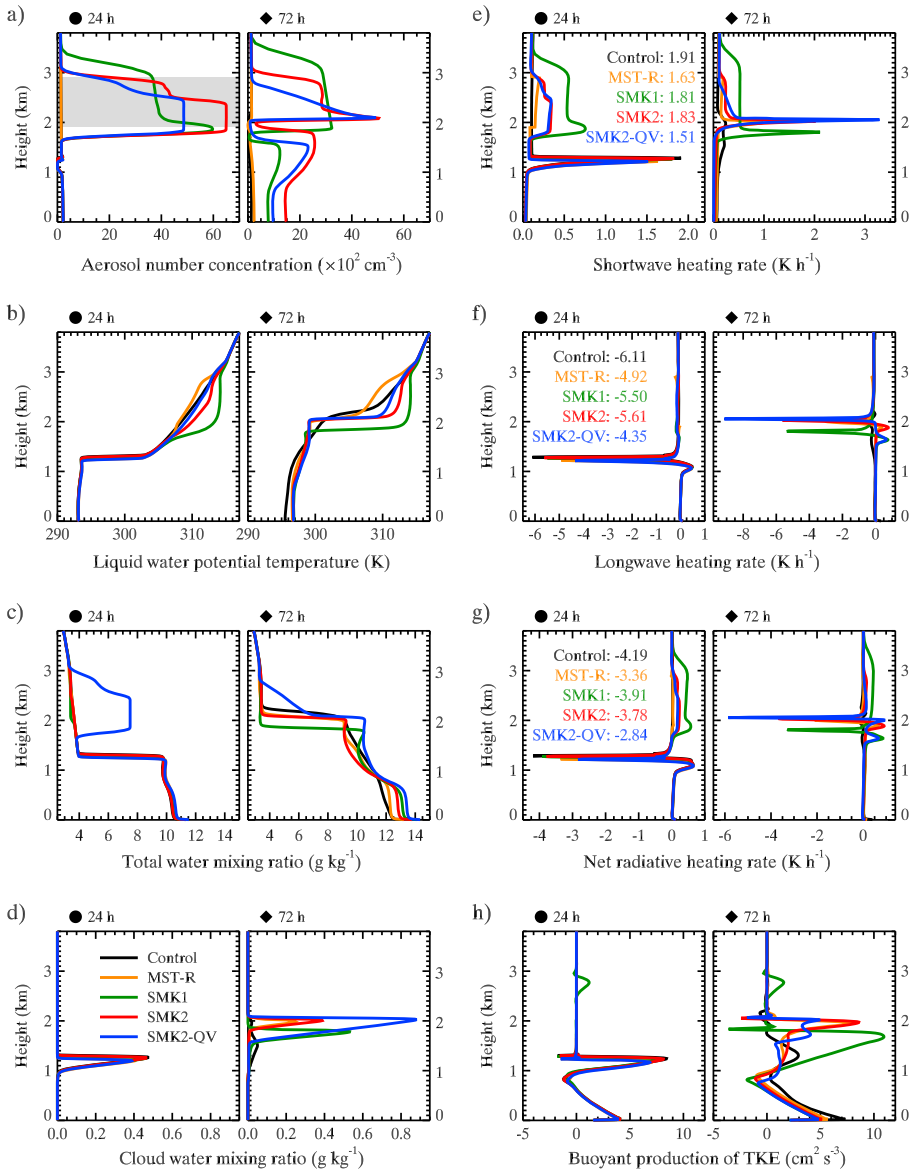

Figure 2. Hourly averaged horizontal mean vertical profiles for five cases for 24th hour (circle) and 72nd hour (diamond). f_c starts declining at 24 h (Figure 1a). The initial smoke/moist layer is shown by the shading in Figure 1a (circle). The mean cloud top heating rates for the 24th hour are listed. Note that different horizontal axis ranges are used for heating rates.

the moisture and optical properties of the elevated smoke layer because cloud is the dominant SW absorber below the smoke layer (the initial $\tau_c \approx 17$). Extinction in the smoke layer above accounts for only a small reduction in the cloud top SW heating. Therefore, it is primarily the moisture in the smoke/moist layer aloft that modifies (reduces) the *net* radiative cooling at the cloud top through LW effects.

The reduced cloud top cooling drives weaker turbulence, and for SMK2-QV and MST-R, the effect manifests in smaller CWP, weaker entrainment, and enhanced daytime evaporation. After 24 h, when the smoke/moist layer is still not in contact with cloud, the cloud top LW cooling and cloud layer TKE_B are reduced (Figures 2f, circle and 2h, circle). The cloud top net radiative cooling is dominated by the LW and is decreased mainly due to the decrease in cloud top LW cooling (Figure 2g, circle). The reduced cloud top cooling further diminishes the source of turbulence and its ability to condense cloud water. The cloud top SW heating is only marginally reduced for the smoke/moist cases (Figure 2e, circle), and the associated additional cloud top cooling is small.

As noted earlier, the increased water vapor amount is larger than typical values for high τ_a for St. Helena soundings [*Adebiyi et al.*, 2015]; thus, the reduction of the cloud top cooling may be excessive for these moist layer simulations.

3.5. Influence of Moisture and Smoke Layer After Contact: SMK2-QV and MST-R; $t > 38$ h

As in the case of SMK1 and SMK2, when the boundary layer reaches the smoke layer, n_c for SMK2-QV increases dramatically, which inhibits rain production (Figures 1d and 1e). While the smoke enhances the inversion strength, moisture counteracts the enhanced stabilization through LW cooling, especially during the night; MST-R is coolest within the moist layer, and SMK2-QV has the weakest stabilization among the smoke cases (Figure 2b, diamond).

The entrainment of the increased moisture for SMK2-QV produces a very large CWP increase during the third night and forms a much thicker nonprecipitating stratocumulus deck with strong cloud top cooling (Figures 1b, 2d, diamond, and 2g, diamond). This results in a faster growth rate of z_i, due to the simultaneously increased TKE and slightly weaker inversion during the third night (Figures 1c, 1f, and 1g). This fast deepening of the boundary layer is similar to the FAST case of SS11, which starts with a weaker inversion jump and larger free tropospheric moisture.

3.6. Dynamical Effect

The dynamical effect of smoke, as expressed by the TKE_B, does not propagate below ~800 m because of decoupling (Figures 2b, 2c, and 2h). Throughout the simulation, the TKE_B profile below the decoupling level (~800 m) does not differ substantially among the cases except in the transitioned Control case. This also appears in the surface fluxes; the sensible heat flux (mean $\approx$ 6.2 W m^{-2}) differs by ~2 W m^{-2} at most among the cases before the transition occurs in Control and MST-R, and the latent heat flux (mean $\approx$ 112 W m^{-2}) differs by ~15 W m^{-2} at most. Thus, smoke mainly exerts its influence above the decoupling level. The dynamical effect of smoke on the turbulence above the decoupling level after smoke is sufficiently entrained is apparent in the TKE_B (Figure 2h, diamond). *Johnson et al.* [2004] found that smoke immediately above builds cloud condensate via enhanced inversion stability, resulting in stronger turbulence, while smoke inside the boundary layer evaporates cloud via increased in-cloud SW heating, leading to weaker turbulence. The state at 72 h for the smoke cases experiences these two competing effects. SMK1 has a linear TKE_B profile above the decoupling level, which indicates a well-maintained stratocumulus due to stronger inversion strength, lower z_i, and moister cloud layer (Figures 2b, diamond and 2c, diamond). Interestingly, SMK2-QV has a weaker in-cloud TKE_B than SMK1 and SMK2, even though SMK2-QV has a thicker stratocumulus layer. Since z_i and its growth rate are similar between SMK2 and SMK2-QV around 72 h (Figure 1c), a possible explanation for this weaker turbulence is the increased in-cloud SW heating associated with smoke and large cloud water amount (Figure 2e, diamond), as well as the reduced cloud top LW cooling because of the presence of enhanced moisture above.

3.7. Radiative Effect

The presence of a smoke layer aloft modulates the SW cloud radiative effect (SWCRE), calculated as $\left(F^{\downarrow}_{\text{all}} - F^{\uparrow}_{\text{all}}\right) - \left(F^{\downarrow}_{\text{clear}} - F^{\uparrow}_{\text{clear}}\right)$, where F is SW flux at the top of atmosphere (Figure 1h). For the given initial thermodynamic profile, the smoke layer weakens the SWCRE in proportion to its absorption of SW. As expected, smaller ω_o (i.e., more absorbing smoke) effectively reduces the amplitude of the SWCRE (Figure 1h for the first few hours when all cases have similar profiles). This weaker SWCRE persists through day 2. In contrast, SWCRE is enhanced when the smoke interacts with cloud ($t > 38$ h), especially for SMK2, which has the largest n_c, by suppressing rain formation and maintaining optically thick clouds and high f_c. After 38 h, relative to Control, SWCRE is enhanced by $\approx$ −44 W m^{-2} for SMK1, $\approx$ −67 W m^{-2} for SMK2, and $\approx$ −86 W m^{-2} for SMK2-QV (daytime average). Calculating the atmospheric component of the radiative effect of the smoke as a residual of SWCRE minus surface SWCRE, the mean (daytime only) atmospheric enhancement relative to Control is $\approx$ 40 W m^{-2} for SMK1, $\approx$ 10 W m^{-2} for SMK2, and $\approx$ 8.6 W m^{-2} for SMK2-QV.

3.8. Timing of SCT

SS11 found that the pace of the SCT is largely determined by the initial LTS. The relative decrease in domain mean albedo, $\Delta A = \frac{A_{0h} - A_{72h}}{A_{0h}}$, a measure of the amplitude of the SCT, is 0.51 for their REF simulation. For our simulations, $\Delta A \approx 0.69$ for Control, ≈ 0.5 for MST-R, ≈ -0.15 for SMK1, ≈ -0.1 for SMK2, and ≈ -0.54 for SMK2-QV. Clearly, through radiative and microphysical modulations the smoke layer slows the rate of the SCT for the conditions considered by increasing LTS and inversion strength and inhibiting precipitation-associated transition. Key physical mechanisms and effects arising in the presence of the moist, smoke layer on SCT are summarized in Figure 3, conveying some of the complexity of the system. Further study is required to assess

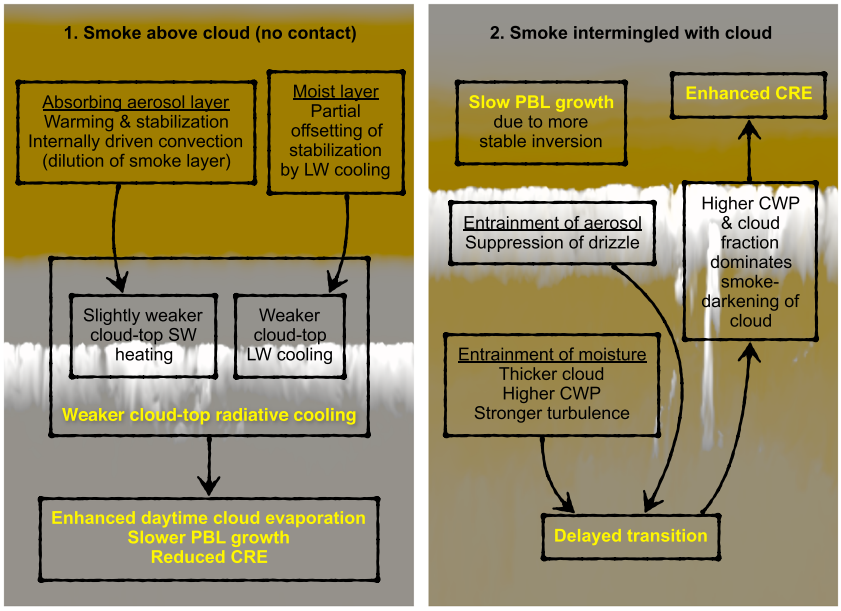

Figure 3. Key effects of smoke and moisture on SCT (left) when the layer is above cloud and (right) when it interacts with cloud.

if the timing of the SCT differs between the dry and the humidified smoke beyond day 3. If indeed the SCT is delayed in the presence of smoke in the South East Atlantic, it would result in a westward extension of the stratocumulus deck, provided that the large scale circulation is unaffected by the smoke. Qualitative observational confirmation of this result appears in *Adebiyi et al.* [2015] who show that the stratocumulus deck extends to ~20°W for polluted conditions, whereas it is limited to ~10°W in the absence of smoke (their Figure 24). Whether this represents a potential climate forcing would depend on the seasonality, frequency of occurrence, and extent of this phenomenon.

4. Conclusions

Smoke in the free atmosphere overlaying, but separated from, the stratocumulus during the transition to cumulus acts in a fundamentally different way on the boundary layer than SST warming. Smoke is a source of heating that varies spatially through progressive dilution and removal and diurnally with the solar zenith angle. In the case of a very strong heating source, smoke-generated convection can help to transport the smoke upward. Through a series of simulations, we have shown that the key mechanisms via which well-mixed boundary layers transition to decoupled boundary layers with penetrative cumulus [*Bretherton*, 1992; *Wyant et al.*, 1997] are modified by smoke.

Smoke overriding the stratocumulus deck has a significant impact on the transition, depending on its proximity to the cloud layer, τ_a and ω_o, and the ambient RH. The primary pathways via which the smoke affects the transition are through modification in the LTS and the inversion strength, suppression of boundary layer deepening and concomitant entrainment, and microphysical suppression of precipitation. When the smoke is accompanied by enhanced humidity, there are profound effects resulting from weakening of cloud top radiative cooling, offsetting effects of smoke SW heating and water vapor LW cooling on stabilization in the smoke layer, and, when vapor is entrained into the cloud, formation of a thicker cloud layer. Modification to cloud top SW heating is a secondary effect.

In addition to the spatiotemporal variability in the smoke, the timing of cloud contact with the smoke layer, both in the diurnal cycle and stage of transition, may be important. This differs from the SCT in the absence of smoke where the rate of transition is mostly set by the strength of the capping inversion or LTS in the stratocumulus state (SS11). In our smoke simulations, the stratocumulus cloud fully recovers at night, and the transition has not occurred after 3 days; instead, the field evolves into a deep decoupled nonprecipitating stratocumulus boundary layer. This scenario might be altered if the smoke layer were to reside at a much higher level without being entrained, e.g., Figure 1a (SMK1 and SMK2) before 38 h hints at a slightly hastened daytime

breakup in cloud, which is reversed once contact with the cloud is made and smoke suppresses precipitation. If contact of smoke layers and stratocumulus is a dominant feature in the South East Atlantic, we expect delayed SCT and a larger westward extent of the stratocumulus deck [*Adebiyi et al.*, 2015], with potential impacts on climate.

The influence of increased moisture is clearer; here our results suggest significant daytime cloud breakup (Figure 1a) when the moist layer is aloft (MST-R or SMK2-QV before 38 h) but full nighttime recovery of f_c. The radiative effects are buffered by thermodynamic and microphysical effects once the moist and smoky layer is entrained into cloud (f_c recovers on day 3 for SMK2-QV). In the absence of smoke, MST-R transitions to cumulus via precipitation much like Control.

This study provides a broad view of the SCT in the presence of elevated smoke layers, but it is far from complete. Clearly, the interaction of myriad processes still need to be fully addressed and quantified, particularly for the range of South East Atlantic conditions. Field campaigns such as CLARIFY, LASIC, and ORACLES will be an important data source and provide opportunities for the community to address and evaluate more fully the effect of biomass burning aerosol on the marine boundary layer cloud and potential implications for aerosol forcing of climate.

Acknowledgments
The authors thank P. Blossey who kindly provided us case configuration files and B. Stevens for the helpful discussions. This work is supported by the NOAA Climate Program Office through the Climate Process Team, by NOAA's Climate Goal, and by the DOE ASR Program grants DE-SC0006972 and DE-SC0008112. Requests for the System for Atmospheric Modeling (SAM) should be directed to M. Khairoutdinov. Both the data and input files necessary to reproduce the experiments with SAM will be made available by the authors upon request.

References

Ackerman, A. S., O. B. Toon, D. E. Stevens, A. J. Heymsfield, V. Ramanathan, and E. J. Welton (2000), Reduction of tropical cloudiness by soot, *Science*, *288*(5468), 1042–1047, doi:10.1126/science.288.5468.1042.

Adebiyi, A. A., P. Zuidema, and S. J. Abel (2015), The convolution of dynamics and moisture with the presence of shortwave absorbing aerosols over the southeast Atlantic, *J. Clim.*, *28*(5), 1997–2024, doi:10.1175/JCLI-D-14-00352.1.

Bretherton, C. (1992), A conceptual model of the stratocumulus-trade-cumulus transition in the subtropical oceans, in *Proceeding of the 11th International Conference on Clouds and Precipitation*, vol. 1, pp. 374–377, Int. Comm. on Clouds and Precipitation and Int. Assoc. of Meteor. and Atmos. Phys., Montreal, Quebec, Canada.

Bretherton, C. S., and P. N. Blossey (2014), Low cloud reduction in a greenhouse-warmed climate: Results from Lagrangian LES of a subtropical marine cloudiness transition, *J. Adv. Model. Earth Syst.*, *6*(1), 91–114, doi:10.1002/2013MS000250.

Feingold, G., R. L. Walko, B. Stevens, and W. R. Cotton (1998), Simulations of marine stratocumulus using a new microphysical parameterization scheme, *Atmos. Res.*, *47–48*, 505–528, doi:10.1016/s0169-8095(98)00058-1.

Feingold, G., H. Jiang, and J. Y. Harrington (2005), On smoke suppression of clouds in Amazonia, *Geophys. Res. Lett.*, *32*, L02804, doi:10.1029/2004GL021369.

Hill, A. A., and S. Dobbie (2008), The impact of aerosols on non-precipitating marine stratocumulus. II: The semi-direct effect, *Q. J. R. Meteorol. Soc.*, *134*(634), 1155–1165, doi:10.1002/qj.277.

Johnson, B. T. (2005), Large-eddy simulations of the semidirect aerosol effect in shallow cumulus regimes, *J. Geophys. Res.*, *110*, D14206, doi:10.1029/2004JD005601.

Johnson, B. T., K. P. Shine, and P. M. Forster (2004), The semi-direct aerosol effect: Impact of absorbing aerosols on marine stratocumulus, *Q. J. R. Meteorol. Soc.*, *130*(599), 1407–1422, doi:10.1256/qj.03.61.

Khairoutdinov, M. F., and D. A. Randall (2003), Cloud resolving modeling of the arm summer 1997 IOP: Model formulation, results, uncertainties, and sensitivities, *J. Atmos. Sci.*, *60*(4), 607–625, doi:10.1175/1520-0469(2003)060<0607:CRMOTA>2.0.CO;2.

Krueger, S. K., G. T. McLean, and Q. Fu (1995), Numerical simulation of the stratus-to-cumulus transition in the subtropical marine boundary layer. Part I: Boundary-layer structure, *J. Atmos. Sci.*, *52*(16), 2839–2850.

Mlawer, E. J., S. J. Taubman, P. D. Brown, M. J. Iacono, and S. A. Clough (1997), Radiative transfer for inhomogeneous atmospheres: RRTM, a validated correlated-k model for the longwave, *J. Geophys. Res.*, *102*(D14), 16,663–16,682, doi:10.1029/97JD00237.

Painemal, D., S. Kato, and P. Minnis (2014), Boundary layer regulation in the southeast Atlantic cloud microphysics during the biomass burning season as seen by the A-train satellite constellation, *J. Geophys. Res. Atmos.*, *119*, 11,288–11,302, doi:10.1002/2014JD022182.

Sandu, I., and B. Stevens (2011), On the factors modulating the stratocumulus to cumulus transitions, *J. Atmos. Sci.*, *68*(9), 1865–1881, doi:10.1175/2011jas3614.1.

Sandu, I., B. Stevens, and R. Pincus (2010), On the transitions in marine boundary layer cloudiness, *Atmos. Chem. Phys.*, *10*(5), 2377–2391, doi:10.5194/acp-10-2377-2010.

Wang, H., G. Feingold, R. Wood, and J. Kazil (2010), Modelling microphysical and meteorological controls on precipitation and cloud cellular structures in Southeast Pacific stratocumulus, *Atmos. Chem. Phys.*, *10*(13), 6347–6362, doi:10.5194/acp-10-6347-2010.

Wang, S., B. A. Albrecht, and P. Minnis (1993), A regional simulation of marine boundary-layer clouds, *J. Atmos. Sci.*, *50*(24), 4022–4043.

Wilcox, E. M. (2010), Stratocumulus cloud thickening beneath layers of absorbing smoke aerosol, *Atmos. Chem. Phys.*, *10*(23), 11,769–11,777, doi:10.5194/acp-10-11769-2010.

Wilcox, E. M. (2012), Direct and semi-direct radiative forcing of smoke aerosols over clouds, *Atmos. Chem. Phys.*, *12*(1), 139–149, doi:10.5194/acp-12-139-2012.

Wyant, M. C., C. S. Bretherton, H. A. Rand, and D. E. Stevens (1997), Numerical simulations and a conceptual model of the stratocumulus to trade cumulus transition, *J. Atmos. Sci.*, *54*(1), 168–192.